Intracellular localization and splicing regulation of FUS/TLS are variably affected by amyotrophic lateral sclerosis-linked mutations

Yoshihiro Kino[1], Chika Washizu[1], Elisa Aquilanti[2], Misako Okuno[1], Masaru Kurosawa[1], Mizuki Yamada[1], Hiroshi Doi[1,3] and Nobuyuki Nukina[1,*]

[1]Laboratory for Structural Neuropathology, Brain Science Institute, RIKEN, 2-1, Hirosawa, Wako-shi, Saitama, 351-0198, Japan, [2]Albert Einstein College of Medicine, 1300 Morris Park Avenue, Bronx, NY 10461, USA and [3]Department of Clinical Neurology and Stroke Medicine, Graduate School of Medicine, Yokohama City University, 3-9 Fukuura, Kanazawa-ku, Yokohama 236-0004, Japan

ABSTRACT

TLS (translocated in liposarcoma), also known as FUS (fused in sarcoma), is an RNA/DNA-binding protein that plays regulatory roles in transcription, pre-mRNA splicing and mRNA transport. Mutations in *TLS* are responsible for familial amyotrophic lateral sclerosis (ALS) type 6. Furthermore, TLS-containing intracellular inclusions are found in polyglutamine diseases, sporadic ALS, non-SOD1 familial ALS and a subset of frontotemporal lobar degeneration, indicating a pathological significance of TLS in a wide variety of neurodegenerative diseases. Here, we identified TLS domains that determine intracellular localization of the murine TLS. Among them, PY-NLS located in the C-terminus is a strong determinant of intracellular localization as well as splicing regulation of an E1A-derived minigene. Disruption of PY-NLS promoted the formation of cytoplasmic granules that were partially overlapped with stress granules and P-bodies. Some of the ALS-linked mutations altered both intracellular localization and splicing regulation of TLS, while most mutations alone did not affect splicing regulation. However, phospho-mimetic substitution of Ser505 (or Ser513 in human) could enhance the effects of ALS mutations, highlighting interplay between post-translational modification and ALS-linked mutations. These results demonstrate that ALS-linked mutations can variably cause loss of nuclear functions of TLS depending on the degree of impairment in nuclear localization.

INTRODUCTION

TLS (translocated in liposarcoma)/FUS (fused in sarcoma) is an RNA/DNA-binding protein implicated in multiple diseases. As its name indicates, chromosomal translocation of *TLS* was found in sarcoma and leukemia and results in the production of an oncogenic fusion protein that consists of the N-terminal portion of TLS and a partner protein such as CHOP and ERG (1–3). The N-terminus region of TLS is rich in Gln, Ser, Tyr and Gly residues (QSYG) and acts as a transcriptional co-activation domain (4). Recently, TLS has been implicated in neurodegenerative disorders. Huntington's disease (HD) is an autosomal dominant disease caused by an expansion of a CAG repeat that encodes a polyglutamine tract in the huntingtin protein. We previously reported that TLS is a protein component of inclusion bodies in HD patients and a model mouse (5). Moreover, TLS is also found in the inclusion bodies of other polyglutamine diseases such as spinocerebellar ataxia (SCA) type 1, 2 and 3 and dentatorubral-pallidoluysian atrophy (DRPLA) (6,7). These results raised a possibility that TLS function is compromised by polyglutamine disease proteins.

More recently, mutations of *TLS* were identified in familial amyotrophic lateral sclerosis (ALS) type 6 (ALS6) and some sporadic ALS patients (8–10). The inheritance of ALS6 is autosomal dominant with the exception of a recessive mutation, H517Q (8–10). The majority of mutations have been identified in exon 15 that encodes the C-terminal end of the protein, where a nuclear localization signal (NLS) is predicted (10,11). Most others are missense mutations located in distinct regions of the open reading frame (10). In ALS6 patients, ubiquitin-positive cytoplasmic inclusions of TLS have been identified (8,9). Furthermore, TLS pathology has been identified in a

*To whom correspondence should be addressed. Tel: +81 48 467 9702; Fax: +81 48 462 4796; Email: nukina@brain.riken.jp

subset of frontotemporal lobar degeneration (FTLD), now classified as FTLD-FUS, which includes atypical FTLD with ubiquitinated inclusions (aFTLD-U), neuronal intermediate filament inclusion disease (NIFID) and basophilic inclusion body disease (BIBD) (6,12–15). These observations indicate that TLS pathology is common to a wide spectrum of brain diseases. Remarkably, this situation was preceded by another RNA-binding protein, TDP-43 (transactive response DNA-binding protein 43) (10). TDP-43 has been identified as a major component of inclusions in sporadic ALS as well as the majority of FTLD with ubiquitin-positive inclusions (FTLD-U) (16). Subsequently, *TDP-43* mutations have been found in ALS and FTLD patients (17,18). TDP-43-positive inclusions were observed in FTLD caused by mutations of other genes such as *GRN* and *VCP* (16,19). Thus, FTLD subtypes with TDP-43-positive inclusions are now categorized as FTLD-TDP (15). Initially, pathological changes of TDP-43 and TLS were thought to be mutually exclusive, and TLS was not expected to be present in the inclusions of FTLD-TDP and most of sporadic ALS (6,10). More recently, however, TLS immunoreactivity was detected in TDP-positive inclusions of sporadic ALS, non-SOD1 familial ALS and FTLD with or without *GRN* mutations (20). Therefore, TLS and TDP-43 are major proteins aberrantly accumulated in a wide range of ALS and FTLD tissues, suggesting common pathogenic pathways between these diseases.

In this context, it is crucial to understand the cause and consequence of TLS mislocalization in the inclusions. It is still unclear whether ALS6 mutations result in a loss or gain of function. TLS regulates various steps of RNA metabolisms including transcription, pre-mRNA splicing and mRNA transport (10). TLS contains three types of RNA-binding motifs, three Arg–Gly–Gly (RGG) boxes (RGG1, RGG2 and RGG3), an RNA recognition motif (RRM), and a zinc-finger motif (ZnF). The ZnF is involved in the binding to RNA containing a GGUG motif, a preferential sequence for TLS (21,22). To date, two independent TLS knockout mouse strains were established (23,24). These models revealed that TLS deficiency causes postnatal lethality in inbred animals, abnormal neuronal morphology, chromosomal instability, sensitivity to ionizing irradiation and male infertility (23–25). However, although an extensive analysis of neurological or behavioral features has not been conducted, heterozygous animals are healthy. Like TLS, TDP-43 is involved in transcription and alternative splicing (26,27). TDP-43 is a nuclear protein and cytoplasmic accumulation of TDP-43 in ALS and FTLD-TDP is accompanied by concomitant depletion of this protein from the nucleus (16), suggesting loss of nuclear functions of TDP-43 in these conditions. Importantly, splicing misregulation of a large number of genes has been reported in sporadic ALS (28). Considering the pathological and functional similarity between TLS and TDP-43 and their common roles in alternative splicing, it is crucial to characterize splicing regulation of TLS. Although few splicing targets of TLS have been identified (29), the adenoviral E1A minigene has been

shown to be a suitable reporter system to study TLS splicing regulatory activity (30–32).

Here we tried to identify factors that determine TLS splicing regulatory activity and its intracellular localization. For this purpose, we established a splicing reporter modified from E1A, which facilitated the functional analysis of TLS. We then examined the effect of ALS-related mutations on the function of TLS and found deficit of splicing regulation in a subset of ALS mutants. We also noticed that post-translational protein modifications can modulate the function of TLS in combination with ALS mutations.

MATERIALS AND METHODS

cDNA clones and constructs

Murine TLS cDNA fragment was amplified by polymerase chain reaction (PCR) from TLS-V5 (5) using a primer pair of BamHI-Tls-Fw and XhoI-Tls-Rv for EGFP-TLS-ext or BamHI-Tls-Fw and XhoI-Tls-stop-Rv for EGFP-TLS and inserted in the BglII-SalI sites of pEGFP-C1 (Clontech). TLS-EGFP was made by inserting the TLS fragment amplified by using BamHI-Tls-Fw and XhoI-Tls-Rv into the BglII-SalI sites of pEGFP-N3 (Clontech). Deletions of TLS were made by PCR. TLS-M9 fragment was amplified using BamHI-Tls-Fw and XhoI-Tls-M9-Rv and inserted in the BglII-SalI sites of pEGFP-C1. E1A minigene fragment was amplified from pCS-MT-E1A, a kind gift from Dr. Moreau-Gachelin (30), by PCR using a primer set of BglII-E1A-Fw and SalI-E1A-Rv. This fragment was inserted in pEGFP-C1 to make EGFP-E1A minigene. E1A/mut12s and E1A/mut13s were made by introducing substitutions of 3′-splice site of 12s and 13s in the context of EGFP-E1A. RFP-fused huntingtin exon 1 constructs (18Qex1-RFP and 108Qex1-RFP) were made by inserting huntingtin fragments cleaved by HindIII and BamHI from pcDNA3.1-tNhtt-17Q-EGFP-NLS or pcDNA3.1-tNhtt-153Q-EGFP-NLS (5) to the HindIII-BamHI sites of pcDNA3 with RFP (33). Due to the instability of CAG repeat, the repeat length of mutant huntingtin fragment was variable. We chose a clone with CAG108 or CAG105 for a mutant fragment. For making NLS-fused constructs, oligonucleotides encoding SV40 NLS (BamHI-NLS-BglII-Fw and BamHI-NLS-BglII-Rv) were annealed and ligated with each other to multimerize NLS and cleaved with BglII and BamHI to eliminate head-to-head ligation products. A ladder of multimerized NLS was resolved by agarose gel electrophoresis and the band corresponding to three copies of NLS was collected. Recovered DNA from the band was inserted into the BamHI site of pcDNA3 with RFP to make pcDNA3/NLS-RFP, the BglII site of pEGFP-C1 to make pEGFP-C1-NLS, or the BamHI site of pEGFP-N3 to make pEGFP-N3-NLS. 18Qex1-NLS-RFP and 108Qex1-NLS-RFP were made by inserting above huntingtin fragments into the HindIII-BamHI sites of pcDNA3/NLS-RFP. For making EGFP-fused huntingtin constructs, huntingtin fragment were amplified using BamHI-Htt-Fw and XhoI-Htt-Rv from 18Qex1-RFP and 108Qex1-RFP, and cleaved by BamHI and

XhoI. The resultant fragments were inserted into the BglII-SalI sites of pEGFP-N3-NLS to make 18Qex1-NLS-EGFP and 105Qex1-NLS-EGFP, or into the BglII-SalI sites of pEGFP-N3 to make 18Qex1-EGFP and 105Qex1-EGFP. G3bp1 and TIAR were amplified from mouse cDNA library. A FANTOM3 clone, G730049H03, encoding Nucleolin (Ncl) was provided from Dr Hayashizaki (34). cDNA fragments of G3bp1, TIAR and Ncl were inserted into the BglII-SalI sites of pEGFP-C1 or pRFP-C1 (35).

RFP-M9M and RFP-Bimax2 were made by inserting annealed oligonucleotides encoding M9M and Bimax2 into the BglII-SalI site of pRFP-C1. For making NES-TLS, NES-encoding oligonucleotides, BspEI-NES-Fw and BglII-NES-Rv, were annealed and inserted into the BspEI-BglII sites of pEGFP-C1 and then TLS was inserted in the BglII-SalI sites. The sequence of oligonucleotides is shown in Supplementary Table S1. All constructs were confirmed by sequencing.

Antibodies and reagents

Mouse anti-myc and Alexa-conjugated secondary antibodies were from Invitrogen; rabbit anti-GFP (598) and rabbit anti-Rck/p54/DDX6 (PD009) were from MBL; mouse anti-CUGBP1 (3B1), goat anti-LaminB (M-20), goat anti-eIF3B (sc-16 377), goat anti-TIAR (C-18, sc-1749) and rabbit anti-eIF2α (FL-315, sc-11386) were from Santa Cruz Biotechnology; rabbit anti-FUS (A300–302A) was from Bethyl Laboratories; mouse anti-G3bp1 (611 126) and mouse anti-TLS (611 384) were from BD Transduction Laboratories; rabbit anti-FUS (HPA008784) and rabbit anti-Nucleolin (N2662) were from Sigma-Aldrich; rabbit anti-eIF4G (#2498) was from Cell Signaling Technology. Rabbit anti-TLS-M and anti-TLS-C were described previously (5). Emetine and leptomycin B were purchased from Sigma-Aldrich. Puromycin, G418 and blasticidin were from Invitrogen. Actinomycin D was from Nacalai Tesque.

Cell culture and transfection

N2a, COS-7 and HeLa cells were maintained in Dulbecco's modified Eagle's medium (DMEM) supplemented with 10% fetal bovine serum. For minigene assays, cells were cultured in 12-well plates and transfected with 0.5 μg of plasmids for protein expression and 0.01 μg of plasmids for the expression of a minigene using Lipofectamine 2000 (Invitrogen) according to the manufacturer's instructions. For western blot and immunocytochemistry, see Supplementary Materials and Methods.

Cellular splicing assay

Transfection and cDNA synthesis from cellular RNA were performed as previously described (35). Transfection efficiency was equivalent among constructs in N2a cells, which was determined by the fraction of EGFP-positive cells (~80%). Minigene fragments were amplified by PCR using a fluorescein isothiocyanate (FITC)-labeled forward primer, FITC-E1A-splicing-ex1-Fw and a non-labeled reverse primer, E1A-splicing-ex2-Rv. For E1A/mut12s and E1A/mut13s minigenes, FITC-GFP-Fw and E1A-splicing-ex2-Rv were used for amplification. The sequence of primers is listed in Supplementary Table S1. PCR products were resolved by 2.5% agarose gel electrophoresis. The fluorescence of PCR products was captured by LAS1000 (FUJIFILM). Intensity of band signals was quantified by Multigauge software (FUJIFILM). For the quantification of E1A/mut12s splicing, the ratio of 9s was calculated as $9s/(9s + 13s) \times 100$.

Determination of nucleocytoplasmic localization of EGFP-tagged proteins

EGFP-tagged constructs were transfected into N2a or COS-7 cells plated in 24-well plastic plates. Twenty-four hours post-transfection, cells were fixed with 4% paraformaldehyde/PBS containing Hoechst 33342 for 30 min and washed three times with PBS. ArrayScanV[TI] High Content Screening Reader (Cellomics) was utilized for fluorescent cell image analysis. Cells were identified by their nucleus stained by Hoechst and EGFP-positive cells were selected. For each EGFP-positive cell, average EGFP intensities inside and outside of the nucleus were quantified. A nucleocytoplasmic index (NCI) was defined as (cytoplasmic intensity per pixel)/(cytoplasmic intensity per pixel + nuclear intensity per pixel). This value ranges from 0 to 1 and a higher value indicates stronger cytoplasmic localization in the cell. In one experiment, at least 150 cells were analyzed for each construct and the average NCI value of the cell population was calculated. The 'average NCI' value shown in the figures are the mean of average NCI determined from at least three replicates. When necessary, cells were treated with actinomycin D (actD) at the final concentration of 10 μg/ml for 6 h.

RESULTS

EGFP-fused TLS protein

We first examined the distribution of endogenous TLS in mouse tissues. TLS was detected predominantly in the nuclei of cells in the cerebral cortex, spinal cord and striatum using multiple antibodies recognizing different regions of the protein (Figure 1A for anti-TLS-C and data not shown). Similarly, intracellular localization of endogenous TLS in mouse neuroblastoma Neuro2a (N2a) cells was detected exclusively in the nucleus using anti-TLS antibodies (Figure 1B and data not shown). We utilized murine TLS that was fused to enhanced green fluorescent protein (EGFP) at the N-terminus of TLS (EGFP-TLS). EGFP-TLS localized in the nucleus in N2a cells, as with the endogenous TLS (Figure 1B). In contrast, when EGFP was fused at the C-terminus of TLS (TLS-EGFP), the resultant protein was localized in both nucleus and cytoplasm with occasional formation of cytoplasmic inclusion-like structures or granules (Supplementary Figure S1A and B). Similar intracellular localization was observed when EGFP was fused to the N-terminus of TLS lacking its own stop codon and an
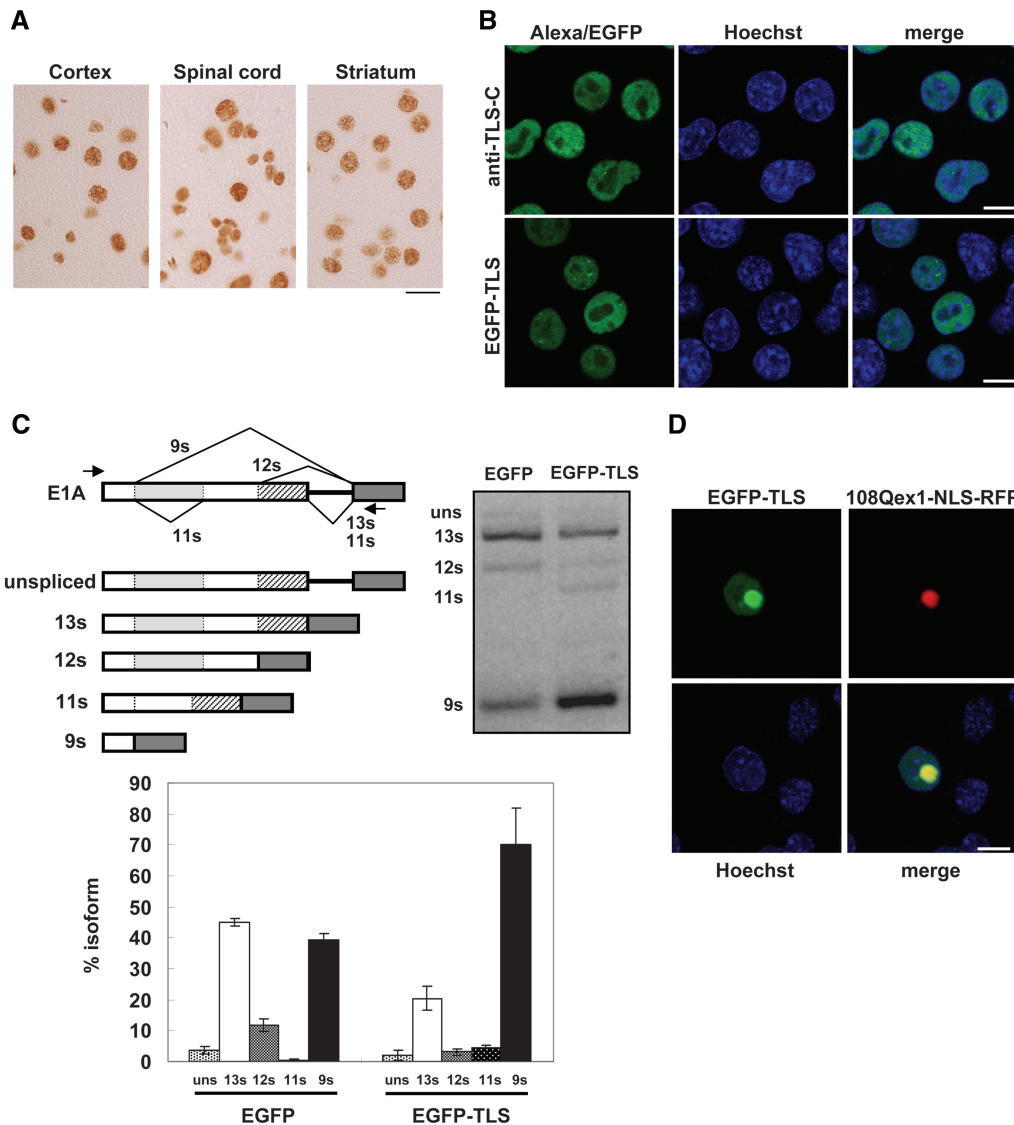
Figure 1. Characterization of EGFP-TLS as a model protein. (**A**) Immunohistochemical analysis of endogenous TLS cerebral cortex, spinal cord and striatum of mouse at the age of 16 weeks. Sections were stained using anti-TLS-C polyclonal antibody. Scale bar represents 20 μm. (**B**) Intracellular localization of endogenous and recombinant TLS in N2A cells. Endogenous TLS was immunostained with a polyclonal antibody against a C-terminal region of TLS and detected by the fluorescence of Alexa 488 conjugated to the secondary antibody (upper panels). EGFP-TLS was transfected into N2a cells and detected by the fluorescence of EGFP (lower panels). Images were obtained by confocal fluorescence microscopy. Hoechst33342 was used for staining the nucleus. (**C**) Structures of the E1A minigene (top left). Spliced and unspliced products are depicted. Splicing assay of E1A minigene of N2a cell transfected with either EGFP or EGFP-TLS (top right). Bottom, quantified results of E1A splicing assay. Bars represent spliced or unspliced products (mean ± SD, *n* = 3). (**D**) Sequestration of EGFP-TLS by huntingtin exon 1 containing 108Q fused with NLS and RFP. Confocal fluorescent images of EGFP and RFP are shown together with nuclear staining with Hoechst 33342. Scale bars in (**B**) and (**D**) represent 10 μm.

extension of l3 amino acids derived from the vector was located at the C-terminus (EGFP-TLS-ext; Supplementary Figure S1A and C). These results suggested that tagging at the C-terminus of TLS can affect its subcellular localization. We next examined the splicing regulatory activity of EGFP-TLS. We utilized the E1A minigene (Figure 1C), a known splicing substrate regulated by TLS (30,32). EGFP-TLS increased the ratio of the shortest spliced product, 9s and decreased both 13s and 12s, consistently with the previous results (32). Finally, as in the case of endogenous TLS (5), EGFP-TLS was sequestered by the inclusion bodies of mutant huntingtin exon 1 fused with monomeric red

fluorescent protein (RFP) (Figure 1D). Similarly, RFP-fused TLS localized in the nucleus as with EGFP-TLS and was sequestered by aggregates of mutant huntingtin exon1 (Supplementary Figure S1D). Thus, EGFP-TLS reproduced previously known features. Based on these results, we decided to use EGFP-TLS as a model protein in the subsequent studies.

Determinants of TLS regions for intracellular localization

We examined a number of deletion mutants of EGFP-TLS to identify the determinants of intracellular localization (Figure 2 and Supplementary Figure S2).

To quantitatively evaluate the localization of the mutants, we measured EGFP intensity in both nucleus and cytoplasm of transfected cells. Relative contribution of cytoplasmic intensity in each cell was represented by a value designated a nucleocytoplasmic index (NCI). NCI ranges from 0 to 1 and a higher NCI indicates stronger cytoplasmic localization of the cell. An average NCI was calculated from the NCI values of all transfected cells of a construct and was used as a simple indicator of localization. For example, EGFP showed an average NCI value around 0.5. The average NCIs of EGFP-nucleolin (nuclear protein) and EGFP-G3bp1 (cytoplasmic protein) were 0.1 and 0.9, respectively (Supplementary Figure S3A).

PY-NLS is a class of NLS that is mediated by transportin/karyopherin β-2 and can be predicted by consensus motifs (11). Interestingly, a previous study predicted a PY-NLS at the very C-terminus of TLS, which directly binds with transportin (11). Consistently, all mutants containing the C-terminus region (amino acids 500–518) localized exclusively in the nucleus (Figure 2 and Grich-PY, RGG2-PY and ZnF-PY in Figure 3A). Interestingly, the full length protein showed exclusion from the nucleoli, whereas other deletions containing the PY-NLS region did not show such exclusion (Figure 3A). This may be determined by the N-terminus QSYG region, as QSYG exhibited nucleoplasmic distribution with nucleolar exclusion similar to the full-length protein, although QSYG was also localized in the cytoplasm (Figure 3A and Supplementary Figure S4A). Next, when a C-terminal region corresponding to exon 15 was deleted, the protein, Δex15, showed enhanced cytoplasmic distribution (Figures 2 and 3B, top panels). Cells with higher expression of Δex15 tended to exhibit small and/or large granular structures (Figure 3B, middle and bottom panels). Thus, PY-NLS promotes nuclear localization and its disruption leads to cytoplasmic accumulation of TLS. Similar cytoplasmic structures were observed in the
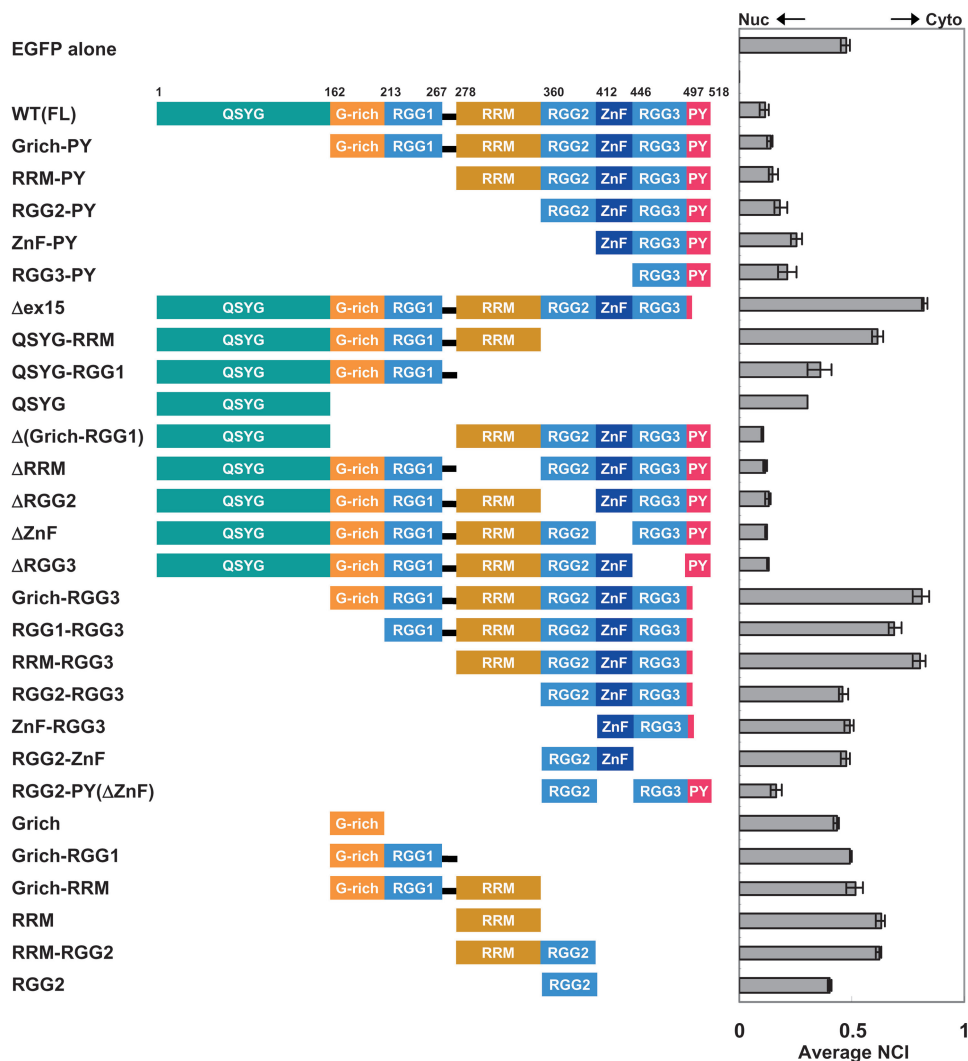

Figure 2. Summary of intracellular localization of EGFP-TLS deletion mutants. Structure and intracellular localization of EGFP-TLS deletion mutants in N2a cells are described. Protein domains of TLS are indicated by colored boxes. Average nucleocytoplasmic index (NCI) values determined for each mutant are shown in the chart (mean ± SD, n = 3).
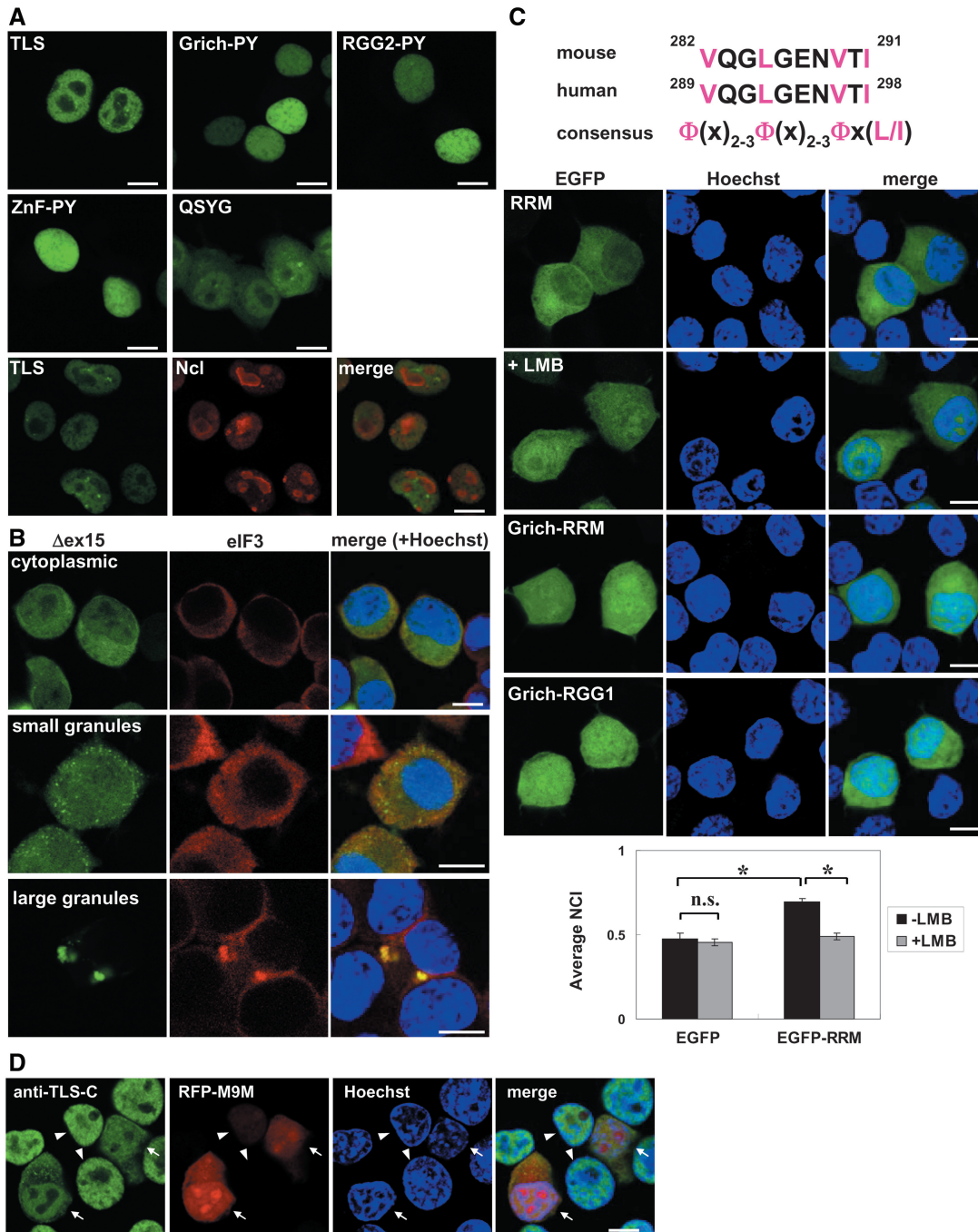
Figure 3. Characterization of PY-NLS and NES of TLS. (**A**) Intracellular localization of N-terminally deleted mutants and QSYG in N2a cells (top and middle panels). Exclusion of EGFP-TLS from the nucleoli immunostained by anti-nucleolin (Ncl) antibody (bottom panels). (**B**) Examples of intracellular localization of the Δex15 mutant. Cells were immunostained by anti-eIF3 antibody (red). (**C**) Confocal images of RRM (with or without leptomycin B treatment), Grich-RRM and Grich-RGG1 fragments. Predicted leucine-rich NES sequences in human and mouse TLS are shown in the top. The consensus sequence of NES is also shown with essential residues in red. Phi represents hydrophobic amino acids, whereas X represents any of amino acids. Bar chart shows the effect of leptomycin B (LMB) treated at 20 nM for 1 h (mean ± SD, $n = 3$). *$P < 0.01$ in ANOVA and Tukey's test. n.s.: not significantly changed. (**D**) Effect of pathway–specific inhibition of nuclear import of TLS. Cells were transfected with RFP-M9M and the localization of endogenous TLS was detected by anti-TLS-C antibody. Arrows indicate cells with higher RFP-M9M expression. Arrowheads indicate cells with little or no RFP-M9M. Scale bars represent 10 μm. Hoechst33342 was used for nuclear staining.

cells expressing TLS-EGFP or EGFP-TLS-ext (Supplementary Figure S1B and C, middle and bottom panels).

Sequence analysis of TLS protein using NetNES1.1 (36) predicted a leucine-rich nuclear export signal (NES) in the RRM region (Figure 3C). Consistently, EGFP-RRM distributed preferentially in the cytoplasm (Figures 2 and 3C). Treatment with leptomycin B, an inhibitor of exportin/CRM1-dependent NES, reduced cytoplasmic accumulation of RRM (+LMB, Figure 3C). Since the

exclusion of RRM from the nucleus was incomplete, the NES activity seemed relatively weak. Interestingly, Grich-RRM did not show cytoplasmic accumulation despite the presence of RRM (Figures 2 and 3C). Since Grich-RGG1 lacking RRM was diffusely distributed throughout the cell and did not promote particular localization (Figure 3C), Grich-RGG1 may negatively modulate the NES activity in the RRM.

Lastly, to directly examine whether disruption of PY-NLS is sufficient for cytoplasmic localization and/or granular formation, we used RFP-fused M9M peptide that specifically binds to transportin and inhibits PY-NLS-mediated nuclear localization (37). Cells with strong RFP fluorescence showed cytoplasmic localization of endogenous TLS (Figure 3D, arrows), with some granular structures. The effect of RFP-M9M seemed to be dose-dependent as cells with weaker or no RFP fluorescence showed normal TLS distribution in the nucleus (Figure 3D, arrowheads). In contrast, TLS was resistant to RFP-fused Bimax2 (Supplementary Figure S4B), an inhibitory peptide against importinα/β-dependent classical NLS (38). A similar observation was found with EGFP-TLS co-transfected with RFP-M9M (Supplementary Figure S4C). These results verified the function and specificity of the predicted PY-NLS.

Cytoplasmic granules of TLS have the characteristics of RNA granules

Previously, TLS was reported to be recruited to stress granules (SGs) in response to stress (39). SG is a cytoplasmic structure thought to act as a triage of mRNA to allow adaptive translation in stressed conditions (40). Larger cytoplasmic granules of Δex15 were colocalized with eIF3 (Figure 3B, bottom panels), which serve as a marker of SGs (41,42). Since the cells were not treated with stress stimuli, this observation indicated that TLS can induce or nucleate stress granules when overexpressed as in the case of TIA-1 and G3BP (40). In contrast, smaller granular structures were not positive for eIF3 immunoreactivity (Figure 3B, middle panels). In N2a cells, small granules were predominant structure. Large eIF3-positive granules were observed in roughly 20% of cells positive for cytoplasmic granules. We then identified the region of TLS essential for cytoplasmic granule formation. Grich-RGG3 and RGG2-RGG3 occasionally showed large cytoplasmic granular structures positive for eIF3 (Figure 4A), while shorter constructs did not efficiently form such structures. The ZnF motif was not an essential region as RGG2-RGG3(ΔZnF) could form eIF3-positive granules (Figure 4B, arrows in upper panels). In addition, RGG2-RGG3(ΔZnF) showed accumulation in the nucleoli (Figure 4B, lower panels), suggesting that the ZnF may inhibit the nucleolar localization of RGG regions. Then, we tested a variant of EGFP-TLS (NES-TLS) in which an NES derived from protein kinase inhibitor alpha (PKI-α) was inserted to enforce cytoplasmic localization without directly disrupting the PY-NLS sequence. NES-TLS exhibited an increased cytoplasmic localization as expected and occasionally formed small and large granules (upper and lower panels, respectively,

in Figure 4C). Thus, cytoplasmic localization, rather than mutation or deletion of PY-NLS itself, is a determinant of granule formation. Cytoplasmic granules were also observed in COS-7 cells. In COS-7 cells, large granules were more prevalent than in N2a and most of cells with cytoplasmic granules were also positive for eIF3 granular staining. In addition to eIF3, other SG markers were colocalized with large, but not small, cytoplasmic granules (Supplementary Figure S5 and Supplementary Data).

SGs are known to be dynamic and their assembly is dependent on the amount of non-polysomal mRNA (43). Emetine is a translational inhibitor that stabilizes polysomes and reduces SGs, whereas puromycin, another translational inhibitor, destabilizes polysomes and facilitates SG formation. SG-like structures of Δex15 were reduced by emetine treatment, while enhanced by puromycin (Supplementary Figure S4D). Finally, we examined the relationship of TLS and P-bodies (PBs), another class of RNA granules associated with mRNA silencing and decay (44). Rck/DDx6 was used as a marker of PBs. Interestingly, some of the small granules of TLSΔex15 showed a partial overlap with PBs (Figure 4D, arrows), whereas other small granules were independent of PBs in N2a cells (Figure 4D, arrowheads). eIF3 showed a diffuse distribution and was not enriched in these TLS small granules (Figure 4D). Remarkably, cells with highly accumulated cytoplasmic TLSΔex15 (~10% of transfected cells) showed only a very small number of PBs (Figure 4E, emphasized by a dashed line in the left bottom panel). This was observed in most cells with eIF3-positive large granules and a fraction of cells with small granules. Such depletion was not observed in cells with high expression of EGFP or EGFP-TLS (data not shown). In COS-7 cells, PBs were often preserved in cells with SG-like large granules (Figure 4F). In these cells, some PBs were located inside of large TLS granules, a pattern not observed in N2a cells (Figure 4Fa). Other PBs were closely located with TLS granules (arrow), or independently distributed in the cell (arrowhead, Figure 4Fb). Depletion of PB could be observed in COS-7 cells, although depletion was less clear than in N2a cells (data not shown). Thus, despite some cell-specific differences, TLS granules are associated with two classes of RNA granules, SGs and PBs. In addition, the appearance of PBs was affected by the overload of cytoplasmic TLS.

E1A minigene variants that facilitate the analysis of splicing regulation

Although the E1A minigene was useful for splicing analysis of TLS, the interpretation of the results was complicated by the multiplicity of splice products. To simplify the analysis of E1A splicing, we tested two variants of E1A that were designed to disrupt one of major spliced isoforms (12s or 13s) by mutating the flanking spliced site (Figure 5A). As expected, both E1A/mut13s and E1A/mut12s minigenes did not show the spliced product corresponding to 13s and 12s, respectively (Figure 5B). When EGFP-TLS was transfected, an
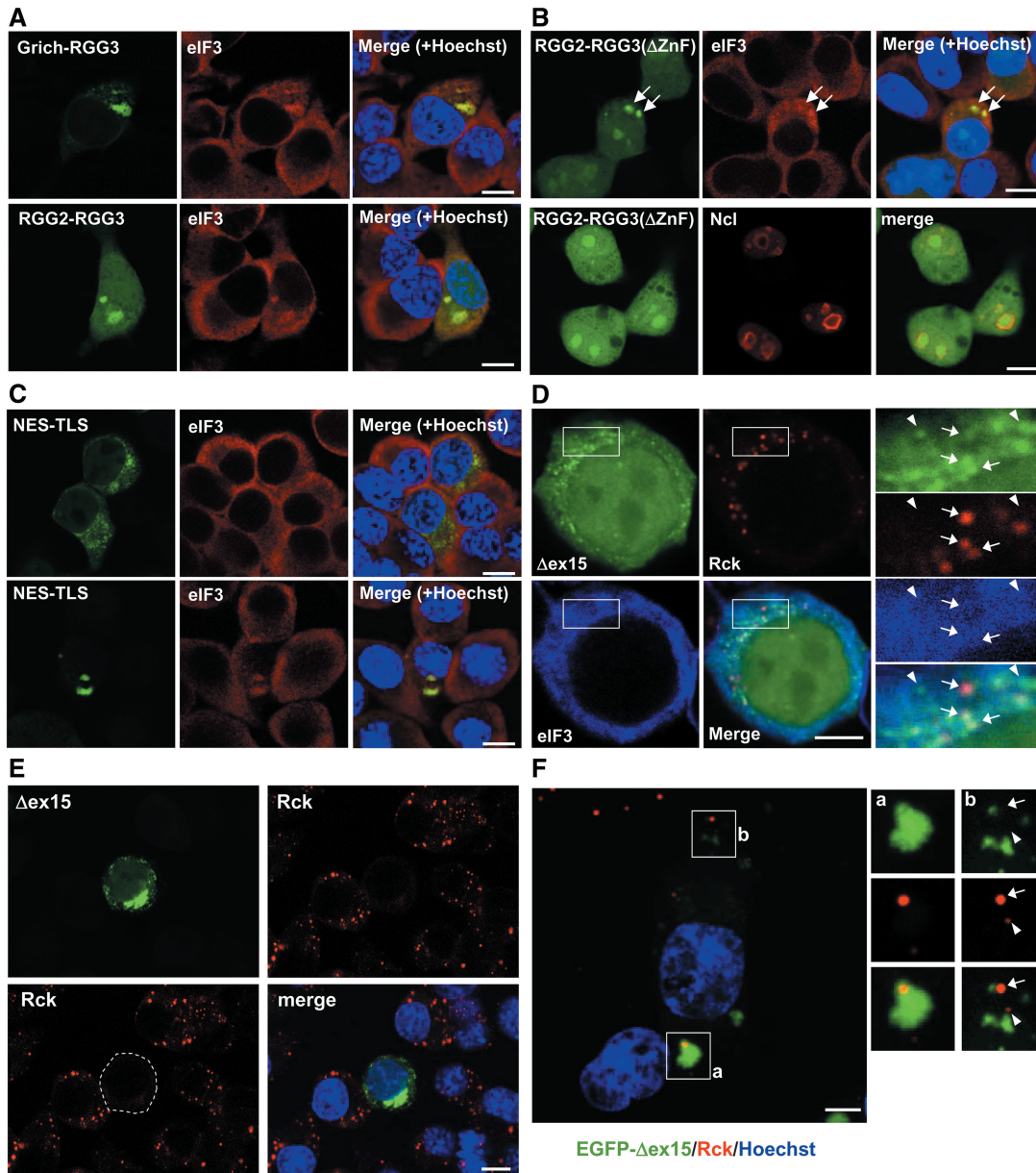
Figure 4. Cytoplasmic localization of TLS. (**A**) Grich-RGG3 and RGG2-RGG3 are sufficient for formation of SG-like large granular structures. N2a cells were immunostained by anti-eIF3 antibody. (**B**) Top panels show the intracellular localization of RGG2-RGG3ΔZnF. The ZnF motif is dispensable for formation of SG-like granules (arrows). Bottom panels show the accumulation of RGG2-RGG3ΔZnF in the nucleolus. Nucleoli were detected by anti-Ncl antibody. (**C**) Cytoplasmic accumulation of NES-TLS. Small (top panels) or large (bottom panels) granules were observed. Large granules were positive for anti-eIF3. (**D**) Partial overlap of TLSΔex15 small granules with PBs in N2a cells. Transfected cells were immunostained with anti-Rck (red) and anti-eIF3 (blue). Right panels are magnified images of the boxed region in the left panels. Arrows indicate TLS small granules overlapped with PBs. Arrowheads indicate TLS small granules not overlapped with PBs. eIF3 was not enriched in TLS small granules. Scale bars represent 10 μm. (**E**) PBs are depleted in N2a cells with higher accumulation of Δex15. PBs were immunostained by anti-Rck. Bottom left panel is identical to top right panel with an exception that the shape of the cell with strong expression of Δex15 is emphasized by a dashed line. Flanking cells without Δex15 fluorescence contain PBs. (**F**) Interaction between large granules of Δex15 and P-bodies. Cells were immunostained with anti-Rck antibody to visualize PBs in COS-7 cells. Magnified images of indicated regions are also shown (a and b). Scale bars represent 10 μm.

increase in 9s was observed with both minigenes (Figure 5B). Therefore, the responsiveness of E1A to EGFP-TLS was retained in these variant minigenes. Since these minigene showed only two major spliced products (9s and either 12s or 13s), these could simplify the splicing analysis. We used the E1A/mut12s minigene for the subsequent studies.

Determinants of TLS splicing activity

We tested TLS deletion mutants in an E1A/mut12s splicing assay to identify TLS domains contributing to splicing regulation. As shown in Figure 5C, deletion of QSYG and Grich-RRG1 and RRM regions did not impair the activity of EGFP-TLS. We then tested
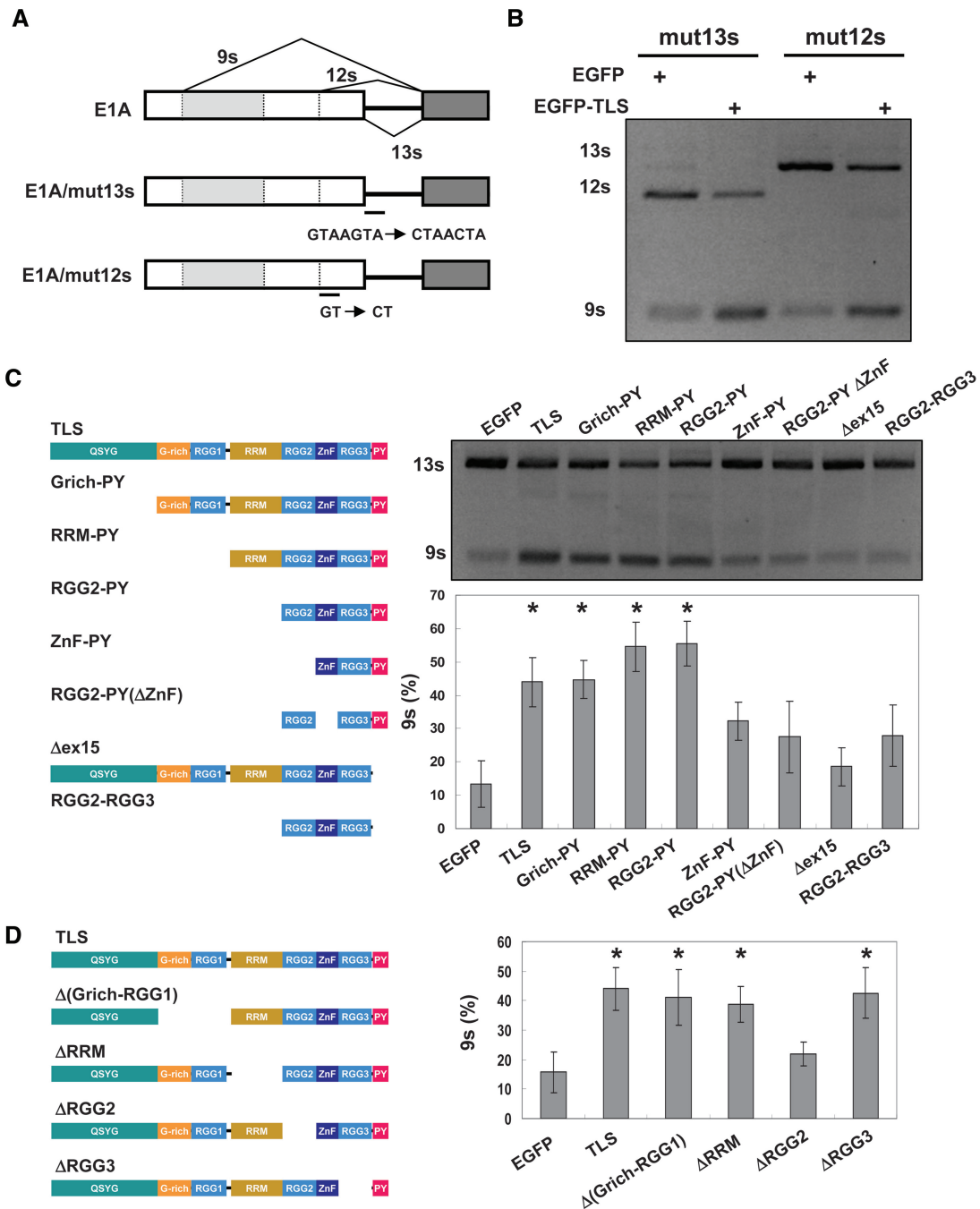
Figure 5. Splicing assay of EGFP-TLS using a variant of the E1A minigene. (**A**) Structure of variant minigenes of E1A. Mut13s and mut12s were made by substation of E1A minigene at the 5′-splice site of 13s and 12s, respectively. (**B**) RT–PCR results of splicing assay using E1A/mut13s and E1A/mut12s in N2a cells. Minigenes were transfected with either EGFP or EGFP-TLS. (**C**) Comparative analysis of TLS deletion mutants using E1A/mut12s. Structures of mutants are shown in the left. Representative gel image of RT–PCR is shown. Bars represent the ratio of the 9s spliced product (mean ± SD, $n = 4$–7). (**D**) Splicing regulation of TLS internal deletion mutants. The structure of mutants is shown in the left. Bar chart shows the results of splicing assay as in (**C**) ($n = 3$–7). *$P < 0.05$, ANOVA and Dunnett's test in comparison with EGFP.

further deletions from RGG2-PY to specify the essential domains. Deletion of any of RGG2, ZnF, or PY-NLS weakened the regulatory activity (Figure 5C). Thus, a C-terminal region from RGG2 to PY-NLS is the minimal region for an optimal splicing regulatory activity. We also tested internal deletions of Grich-RGG1, RRM, RGG2 or RGG3. Deletion of

RGG2, but not the other regions, reduced the activity of EGFP-TLS (Figure 5D). Although the level of protein expression was variable among constructs, this could not explain the difference of splicing activity because all proteins showed protein expression equivalent to or higher than TLS (Supplementary Figure S6A and B). In conclusion, two RNA-binding motifs, ZnF and RGG2

and the PY-NLS are essential for the splicing regulation by TLS.

Although the contribution of PY-NLS to the splicing regulation was reasonable, it was not excluded that the C-terminal region overlapped with another functional motif involved in the splicing regulation. We examined a mutant of TLS (TLS-M9) in which the PY-NLS of TLS was substituted by that of hnRNP A1, known as M9NLS (Supplementary Figure S7A). This substitution changed most residues in the C-terminal region. TLS-M9 was indistinguishable from TLS in both subcellular localization and splicing regulation (Supplementary Figure S7B and C). Thus, the role of the C-terminal region in the splicing regulation was sufficiently explained by the nuclear localization activity of PY-NLS.

The effect of ALS-associated mutations on intracellular localization

We next examined the effect of ALS-linked mutations on murine TLS activity and localization (Figure 6A). We first tested the intracellular localization of TLS mutants in N2a cells (Figure 6B and Supplementary Figure S8). Remarkably, K502E, R514G and P517L showed strong cytoplasmic localization (Figure 6B and red bars in C). All these residues were included in the consensus residues of PY-NLS (residues in red in Figure 6A) that was predicted previously (11). Other mutations were not significantly different from wild-type TLS except for a small increase in average NCI of R506G (Figure 6C). However, a detailed analysis of NCI distribution revealed that H509P, R510K, R513G and R516S showed a small increase in the fraction of cells with NCI greater than 0.1 when compared to wild-type TLS (Supplementary Figure S3B). Interestingly, R506G, H509P and R513G showed clear increase in average NCI in COS-7 cells (Supplementary Figure S3C). We tested several drugs and found that actinomycin D (ActD), a transcription inhibitor, enhanced cytoplasmic localization of wild-type TLS in N2a cells (Figure 6C). Strikingly, however, all C-terminal mutants showed higher cytoplasmic localization compared to wild-type TLS in the presence of ActD (Figure 6C, gray bars). ActD did not alter the localization of EGFP alone (data not shown). Thus, localization of the C-terminal mutants was variable and dependent on cell types and cellular conditions. In contrast, N-terminal mutations did not cause major changes in nucleocytoplasmic distribution of TLS.

Cytoplasmic TLS formed large and small granular structures as observed for TLSΔex15 and NES-TLS (Figure 6D–F and Supplementary Figure S8). For example, P517L showed cytoplasmic accumulation with some large granules colocalized with eIF3 (Figure 6D). Small granules of P517L were occasionally colocalized with PBs but not with SGs (Figure 6E and Supplementary Figure S4E). Most notably, cells with a massive accumulation of P517L had fewer PBs as in the case of Δex15 (Figure 6F). We prepared cells strongly expressing EGFP-P517L using fluorescence-activated cell sorting (FACS) to enrich PB-depleted cells. In a western blot analysis, the level of Rck was not decreased in P517L-expressing cells compared to corresponding cell populations of EGFP or EGFP-TLS (Supplementary Figure S4F), suggesting that the observed loss of PBs by P517L was likely due to redistribution of Rck rather than its reduction.

To exclude that EGFP-tag in the N-terminus affected the localization of TLS, we examined the localization of tag-free TLS with or without ALS mutations. We utilized an N2a-derived cell line stably expressing artificial microRNA (miRNA) that effectively silenced the endogenous TLS (TLS-KD cells, Supplementary Figure S9A and B). TLS(res) was designed to be resistant to the miRNA-mediated RNAi because of substitutions in the region targeted by the miRNA (Supplementary Figure S9C). TLS(res) without any tag was transfected into the TLS-KD cells, which allowed specific detection of TLS(res) by anti-TLS antibodies. Subcellular localization of tag-free TLS(res) and its mutants was consistent with that of EGFP-fused ones (Supplementary Figure S9D). In addition, human tag-free TLS with P525L mutation (corresponding to P517L in mouse) showed intracellular localization similarly to the mouse counterpart (Supplementary Figure S9E).

The effect of ALS-linked mutations on E1A splicing

Since some of ALS-linked mutations altered the localization of TLS, it was expected that these mutations affect splicing regulation as well. Although other mutations did not affect subcellular localization, we thought they could affect splicing by disrupting protein–RNA or protein–protein interactions even with normal nuclear localization. We examined the effect of ALS-linked mutations on the splicing regulatory activity of EGFP-TLS. Among the TLS mutants examined, K502E, R514G and P517L exhibited aberrant regulation of E1A/mut12s splicing (Figure 7A). This was not due to decreased protein expression of these mutants (Figure 7B). Rather, these mutants showed a non-significant tendency towards increased protein levels. All the other mutations did not significantly affect splicing regulation (Figure 7A), consistent with their predominant localization in the nucleus (Figure 6B and C). Thus, there was a clear correlation between mutations of PY-NLS consensus sequence (Figure 6A, residues in red) and deficits in splicing (Figure 7).

Phospho-mimetic substitution at Ser505 modulates the effects of ALS-linked mutants

As demonstrated in Figure 6, intracellular localization of TLS mutants could be dependent on the context including protein environment and/or modifications. We noticed that Ser505 (Ser513 in human) located in the PY-NLS region is a potential phosphorylation site of multiple kinases including CK2, DNA-PK, GSK3, PKC, PKR and others, which were predicted by Group-based Phosphorylation Scoring Method (45). We introduced a phospho-mimetic mutation of S505D in EGFP-TLS and some of the mutants. Although S505D itself did not alter the nucleocytoplasmic distribution of wild-type TLS, this substitution clearly enhanced cytoplasmic localization of G499D, H509P, R510K, R513G and R516S in both N2a
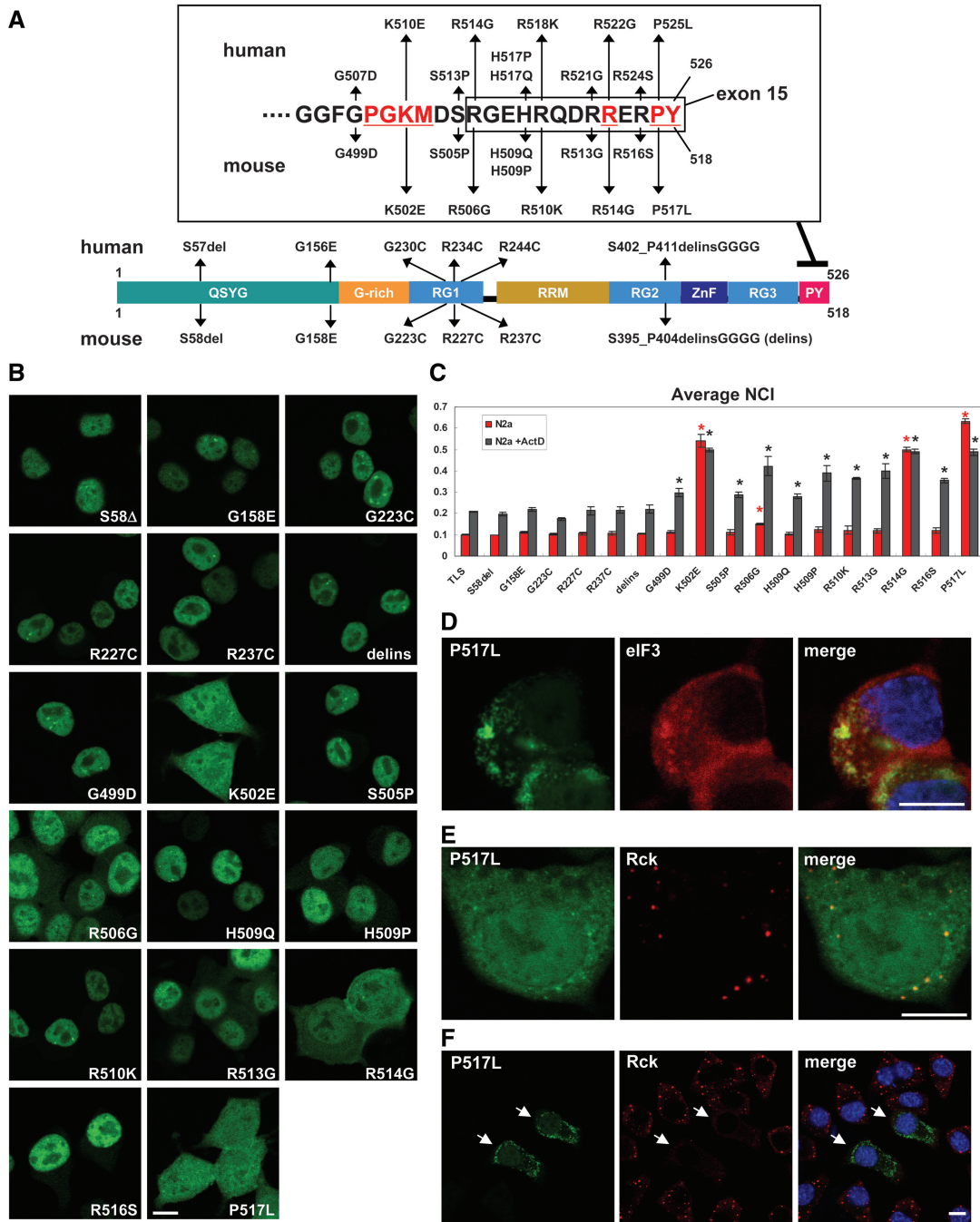
Figure 6. Intracellular localization of ALS-linked mutants of EGFP-TLS. (**A**) ALS-linked mutations examined in this study. Mouse TLS mutations corresponding to known human mutations are indicated. Consensus residues of PY-NLS are shown in red and underlined. Residues encoded by exon 15 are boxed. (**B**) Intracellular localization of EGFP-TLS harboring above mutations in N2a cells. (**C**) Bars represent the average NCI (mean ± SD, $n = 3$) of ALS-linked mutants in untreated N2a cells (red bars) or actinomycin D-treated N2a cells (gray bars). *$P < 0.05$ in ANOVA and Dunnett's test in comparison with TLS. Red and dark asterisks indicate significant difference from TLS in the absence and presence of ActD, respectively. (**D**) An example of cytoplasmic granular structures formed by TLS mutants. (**E**) Partial colocalization of EGFP-P517L and PBs. EGFP-P517L showed partial colocalization with granules immunoreactive with anti-Rck. (**F**) Cells with higher expression of EGFP-P517L (arrows) showed a reduced number of PBs. PBs were immunostained by anti-Rck antibody. Scale bars represent 10 μm in (B, D, E and F).

and COS-7 cells (Figure 8A). In contrast, the distribution of S505D/H509Q was not different from H509Q in these cells (Figure 8A). Although H509Q and H509P are mutations of the same residue, the effect of S505D on these mutants were dramatically different (Figure 8A and B).

We also tested splicing regulatory activity of these mutants. While S505D and S505D/H509Q exhibited normal splicing regulation of E1A/mut12s, S505D/H509P and S505D/R510K showed an impaired regulation with a greater extent for S505D/H509P (Figure 8C).
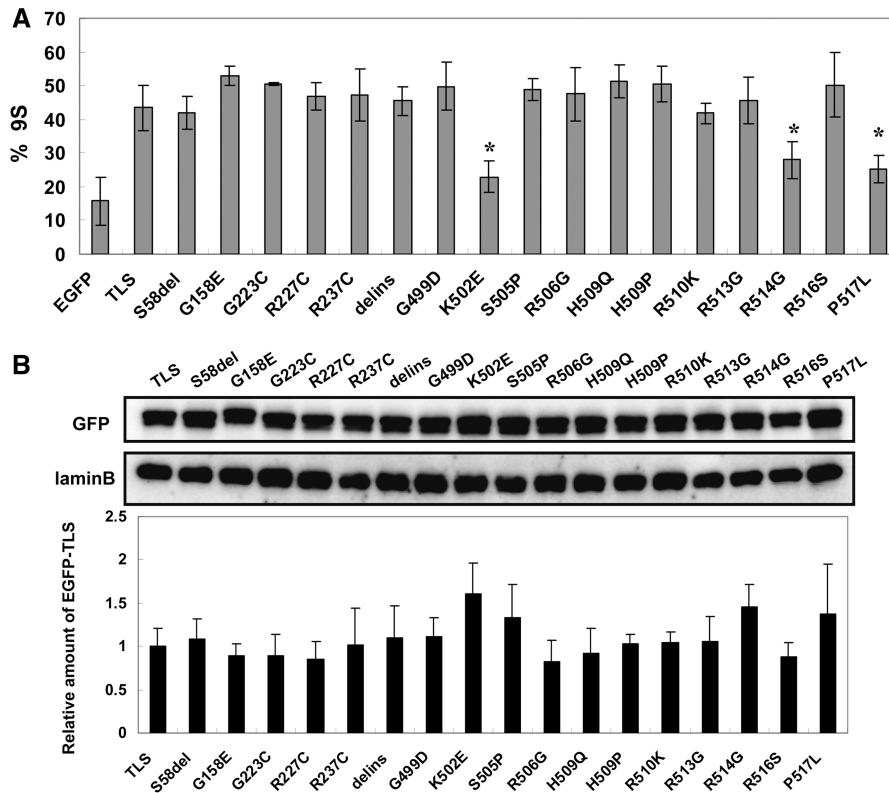
Figure 7. Splicing regulation of ALS-linked mutants of EGFP-TLS. (**A**) Quantification of splicing assay results using E1A/mut12s. Bars represent the ratio of 9S (mean ± SD). All TLS mutants except for K502E, R514G and P517L exhibited statistically significant difference from EGFP ($P < 0.01$), while K502E, R514G and P517L were different from wild-type TLS (*$P < 0.01$, ANOVA and Tukey's test. $n = 4$–7). (**B**) The expression levels of TLS mutants. EGFP-TLS mutants were detected using anti-GFP antibody in a western blot analysis. Bar chart shows the relative protein levels of wild-type or mutant EGFP-TLS that were normalized by LaminB (mean ± SD, $n = 4$). No significant difference from the wild-type was detected by ANOVA and Dunnett's test. G158E reproducibly showed slightly slower migration compared to the others.

Protein levels of these two mutants were not decreased compared to others (Supplementary Figure S6C). Thus, the effect of ALS-linked mutations in the C-terminus could be enhanced by phosphorylation at S505, although this effect was dependent on individual mutations.

DISCUSSION

Identification of *TLS* mutations in ALS raises the question of whether these mutations result in gain or loss of function of the protein. *TLS* mutations were found in multiple regions in the gene. In addition, TLS pathology has been identified in FTLD and ALS patients even without *TLS* mutation. These observations emphasize the importance of understanding the determinants of the TLS function and localization. Here, we identified multiple structural determinants of TLS and provide the first evidence for the effect of ALS-linked mutations on a nuclear function of TLS.

Determinants of intracellular localization and splicing regulatory activity of TLS

By an extensive deletion analysis, we have identified TLS domains that determine the intracellular properties of TLS (Figure 9A). First, a previously predicted PY-NLS located

in the C-terminus was verified by the sensitivity to a specific inhibitor, M9M. In addition, the effect of PY-NLS mutations was stronger when the consensus residues were mutated (Figure 6C). Since all TLS deletion mutants containing PY-NLS were always localized exclusively in the nucleus (Figure 2), PY-NLS is a dominant determinant of localization. Second, an NES was predicted and functionally verified by a specific inhibitor, leptomycin B (Figure 3C). Remarkably, the Grich-RGG1 region was found to suppress cytoplasmic accumulation of RRM, suggesting a context-dependent activity of the NES. Third, QSYG in the N-terminus showed accumulation in the nucleoplasm and exclusion from the nucleolus. On the other hand, RGG2 and RGG3 showed a propensity to accumulate in the nucleoli, which was suppressed by the presence of ZnF. RGG2 and RGG3 may be involved in the nucleolar localization of TLS upon inhibition of RNA polymerase II (46). However, in normal state, this effect seems to be suppressed by ZnF (or perhaps by mRNA-binding) and antagonized by the QSYG region. Interestingly, TLS was found to be a component of Drosha-DGCR8 complex associated with miRNA processing and nucleolar compartment (47,48). However, TLS may not be an essential component of miRNA biogenesis as TLS-KD cells could maintain miRNA-mediated gene silencing despite a severe

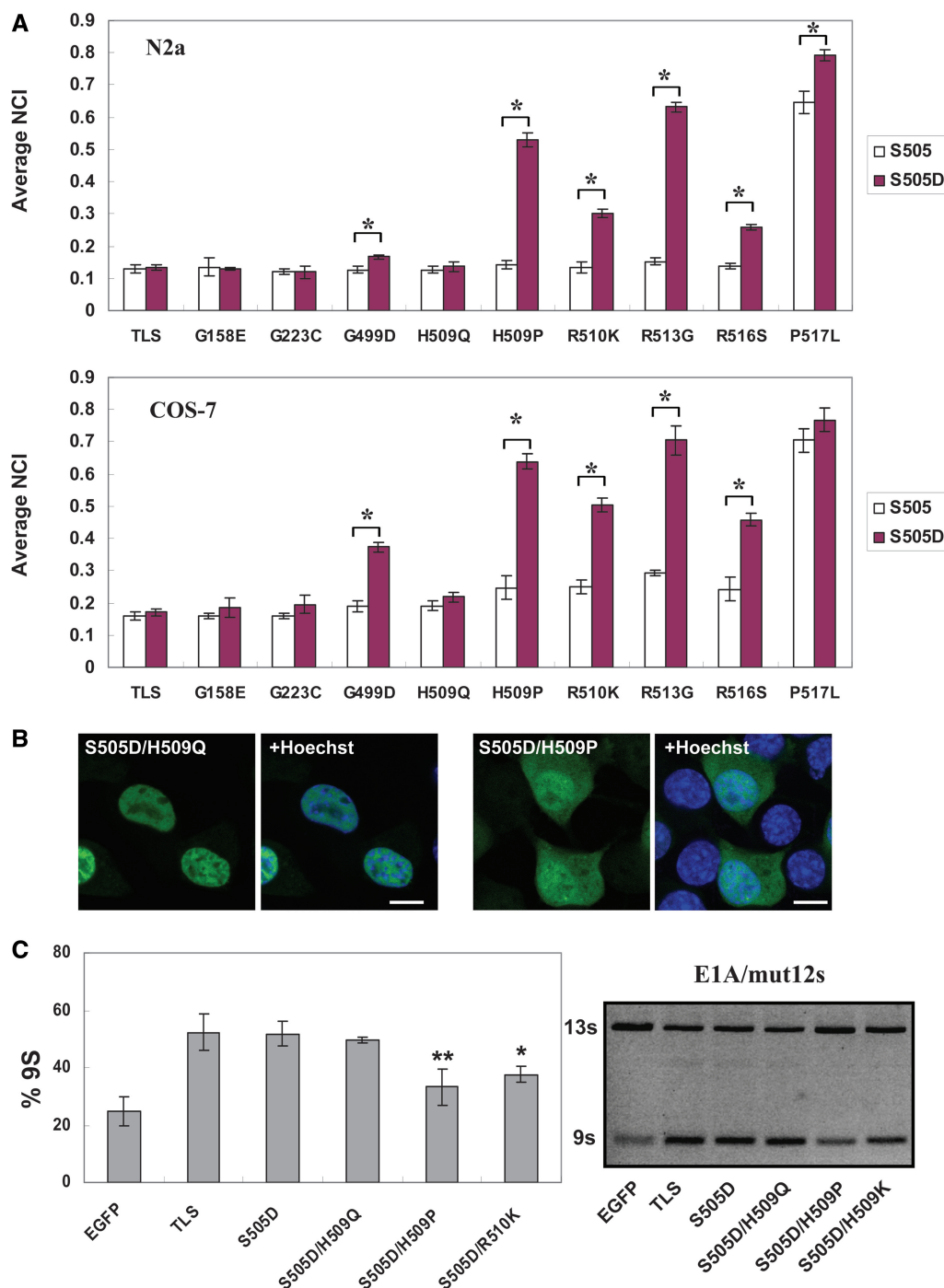**Figure 8.** Phospho-mimetic substitution at Ser505 variably enhances the effects of ALS-linked mutations. (**A**) Intracellular localization of TLS and its mutants with or without S505D substitution in N2a (top) or COS-7 (bottom) cells. Bars represent average NCI values (mean ± SD, $n = 3$). For each mutant, open and red bars indicate non-substituted S505 and S505D, respectively. $*P < 0.05$ in comparison with S505 in two-tailed t-test. (**B**) Intracellular localization of S505D/H509Q (left panels) and S505D/H509P (right panels) in N2a cells. Scale bar indicates 10 μm. (**C**) S505D substitution modulates splicing regulation of E1A/mut12s in N2a cells. Bars represent the ratio of the 9s spliced product as in Figure 5 (mean ± SD, $n = 3$). TLS, S505D and S505D/H509Q showed significantly higher ratio of 9s compared to EGFP ($P < 0.05$). On the other hand, S505D and S505D/ H509Q was not significantly different from TLS. In addition, S505D/H509P and S505D/R510K showed significantly decreased activity compared to TLS, with a greater extent for S505D/H509P (**$**P < 0.01$ and $*P < 0.05$, ANOVA and Tukey's test).

depletion of TLS (Supplementary Figure S9A). Finally, RGG2, ZnF and PY-NLS were found to be essential for splicing regulation of TLS. The former two motifs may play a role in RNA-binding and the PY-NLS increases the nuclear concentration of TLS, which may

synergistically facilitate splicing regulation. Thus, these results revealed not only the localization of TLS subregions but also potential interactions among multiple domains. In this regard, it is interesting that the N-terminus and C-terminus of TLS binds to each other,
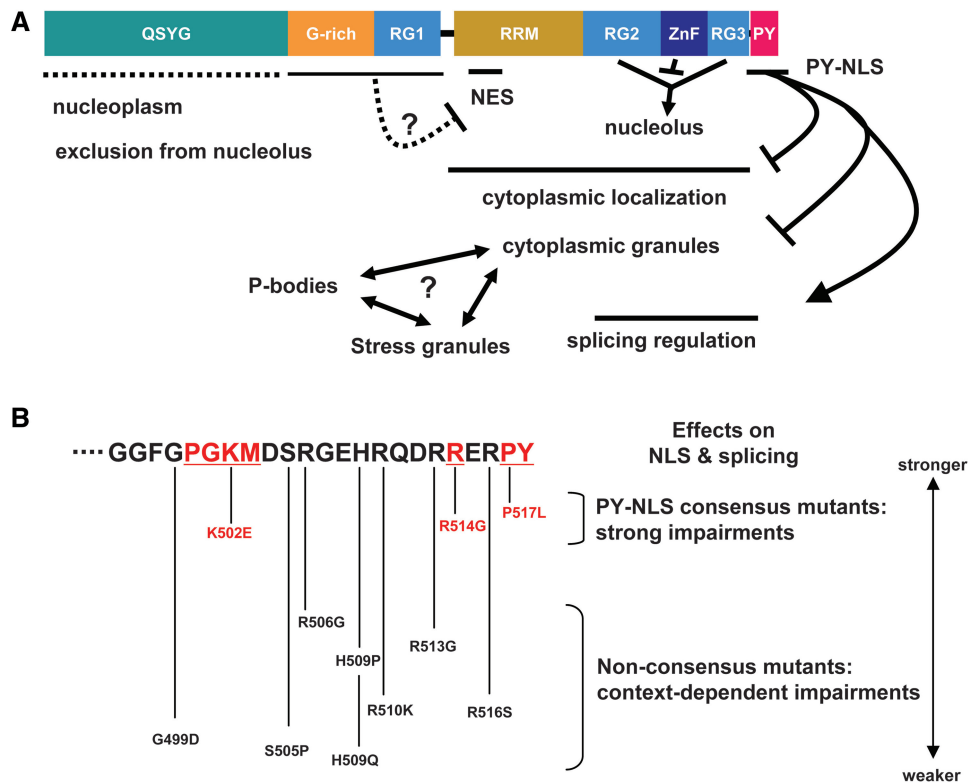
Figure 9. Structural determinants of the properties of TLS and the effects of C-terminal ALS-linked mutations. (**A**) Roles and interplays of TLS internal domains. The effects of each domain found in this study are depicted. See discussion for detail. (**B**) Classification of C-terminal ALS mutations. C-terminal mutations could be clearly divided into two groups, PY-NLS consensus mutations and non-consensus mutations. The order of the effects among mutants was based on Figures 6C, 8A, Supplementary Figure S3B and C. The sequence of the PY-NLS region is shown as in Figure 6A.

and this interaction is allosterically regulated by RNA (49). In addition, several post-translational modifications of TLS have been identified and some of them can modulate the intracellular localization or nucleic acid binding of TLS (50–54). Taken together, complex interactions and regulations among multiple subregions of TLS through RNA-binding and/or post-translational modifications might underlie the multifunctional aspects of TLS.

In this study, we utilized EGFP-fused TLS, which faithfully reproduced nuclear localization of TLS. In contrast, TLS-EGFP lost exclusive nuclear localization (Supplementary Figure S1). This was not simply because of the size of EGFP as a tag, since a similar effect was observed with EGFP-TLS-ext containing an extension of only 13 amino acids (Supplementary Figure S1). It is unusual that C-terminal extension or tagging affected the function of PY-NLS, since this motif can be found in internal regions of other proteins. One possibility is that the C-terminal residues used in this study (Supplementary Figure S1) are specifically incompatible with the PY-NLS. Alternatively, PY-NLS of TLS might have to be located at the end of the protein.

Variable effects of ALS-linked mutations

In this study, we utilized the murine TLS protein and its mutants. This may be suboptimal for understanding TLS in the context of human disease. However, TLS is a highly conserved protein and the key molecular features of TLS are expected to be conserved. In particular, the C-terminus region is perfectly conserved. In addition, the analysis of murine protein is directly relevant to the studies using mouse tissues and genetic models.

Series of experiments clearly demonstrate that PY-NLS function is tightly correlated with not only nuclear localization but also splicing regulation. The effects of ALS mutations on splicing could not be attributed to altered expression level or functional motifs in the C-terminus other than PY-NLS (Figure 7B and Supplementary Figure S7). One clear conclusion is that among the mutations in the PY-NLS region, those that alter the consensus residues of PY-NLS affect both localization and splicing much more strongly than others. In contrast, the other mutations in the C-terminus exhibited more variable effects, which are highly dependent on the context including cell types, conditions and protein modifications (Figures 6C, 8A, B and Supplementary Figure S3C). For example, we observed little or no difference in both localization and splicing regulation between H509Q and H509P in N2a cells (Figures 6B, C and 7A). Despite the mutation of the same residue, H509P showed dramatically stronger effects on both cytoplasmic localization and splicing regulation than H509Q when combined with S505D substitution (Figure 8). This is of interest because their human counterparts H517Q and H517P are associated with recessive and dominant inheritance,

respectively, correlating PY-NLS function or splicing regulation with the mode of inheritance. Another interesting finding is that all C-terminal mutants including H509Q showed an enhanced cytoplasmic localization compared with wild-type in the presence of ActD (Figure 6C). The difference of the effects between ActD and S505D (Figures 6C and 8A) suggests that the effect of ActD may involve a mechanism other than S505 modification. Based on the results of localization and splicing regulation, we classified C-terminal mutations as shown in Figure 9B. We speculate that the effects of ALS-linked mutations may be maximized in some cell type(s) of spinal cord depending on cellular conditions. These results verify that C-terminal mutations can cause an aspect of loss of nuclear function of TLS. It is interesting to examine whether splicing misregulation is observed in ALS6 patients as in sporadic ALS (28). In addition, other nuclear functions of TLS such as transcriptional regulation might be also affected by the disruption of PY-NLS. S505D and possibly other modifications may alter the affinity between PY-NLS and transportin together with ALS-linked mutations. Currently, some of post-translational modifications of TLS were reported to alter the properties of TLS, though the phosphorylation of S505 has not been identified (50–52). Arginine methylation is of interest as it can promote nuclear exclusion of EWS, a paralog of TLS (55,56).

We found that non-C-terminal mutations showed no effects on localization or splicing regulation. Lack of mislocalization was not due to the EGFP tag in the N-terminus, since tag-free non-C-terminal mutants were also localized exclusively in the nucleus (Supplementary Figure S9D). In addition, S505D did not enhance the effect of these non-C-terminal mutations (Figure 8A). Currently, there are some possibilities regarding the effect of non-C-terminal mutations on TLS function. The non-C-terminal and C-terminal mutants might cause some specific deficits other than splicing regulation. Alternatively, non-C-terminal mutations might involve a distinct pathogenic pathway from C-terminal mutations. In both cases, it is also possible that some post-translational modification other than S505 phosphorylation and/or some specific cellular condition including cell types are required for the pathological effects of non-C-terminal mutations.

Cytoplasmic granules of TLS

Mutations that affect PY-NLS resulted in the formation of cytoplasmic granules that include SG-like structures. Although SGs are induced by various stresses as indicated by the name, more than 10 proteins are known to nucleate or induce SGs by themselves when overexpressed (40). Although the physiological and pathological significance of protein-induced SG formation is not well understood, this may cause not only cytoplasmic sequestration of TLS but also reorganization of intracellular ribonucleoprotein complexes and alter mRNA metabolisms. Indeed, the integrity of PBs was affected in cells with massive cytoplasmic accumulation of TLS as determined by the localization of Rck, an essential component of PBs (57).

Thus, TLS mutants could have an aspect of gain of function, in which the interactions and flux of RNA-binding proteins and mRNA are misregulated. Remarkably, basophilic inclusions found in BIBD patients are positive for SG markers such as TIA-1 and PABP and also contain TLS, highlighting the relationship between TLS inclusions and SGs (14,58). In addition to SGs, we observed smaller cytoplasmic granules of TLS partially colocalized with PBs, although many small granules were negative for both anti-eIF3 and anti-Rck. It is possible that these small granules are immature SGs and occasionally fused or docked with existing PBs (59). For future analyses, these RNA granule-like structures must be investigated in neurons since TLS is a component of neuronal granules involved in mRNA transport (60–62). Such cytoplasmic fraction of TLS with or without mutations may be predisposed to the assembly of SGs.

During the article preparation, a paper with closely related subjects was published (63). In agreement with our results, nuclear localization of HA-tagged human TLS in HeLa cells is altered depending on the mutation in the PY-NLS, while non-C-terminal mutations do not affect nuclear localization. In addition, ALS-linked mutations facilitate recruitment of TLS into SGs (63). Although our results are consistent with the report, one experimental difference is that in their study recruitment of TLS into SGs required stress treatment. The discrepancy can be because of the cell type utilized. Consistent with their results, we hardly observed SG-like granules of our TLS constructs in HeLa cells (data not shown). In contrast, SG-like granules were easily observed in COS-7 cells, suggesting the importance of the cell type. In this regard, it is important to note that our P517L construct could form cytoplasmic granules in primary cortical neurons (unpublished data). Furthermore, we also tested tag-free P517L mutant and its human counterpart in N2a cells and observed cytoplasmic granules (Supplementary Figure S9D and E). Therefore, the formation of cytoplasmic granules is not an artifact of EGFP-tagging and could be a common feature of human and mouse TLS.

In conclusion, ALS-linked mutations variably disrupt not only PY-NLS but also splicing regulation and their effects are enhanced by post-translation modifications such as phosphorylation. ALS-linked mutations could be classified into three groups, PY-NLS consensus mutations, non-consensus C-terminal mutations and non-C-terminal mutations. Currently, the effects of non-C-terminal mutations are unclear. Therefore, an important next step is to determine the protein modification of TLS and analyze their effects in combination with ALS-linked mutations. In addition, it is indispensable to characterize neuropathological and clinical genotype–phenotype correlation in patients with TLS mutations, especially for non-C-terminal mutations. Lastly, our results emphasize the importance of understanding the mechanism of RNA granule metabolisms, as TLS is involved in the regulation of both SGs and PBs. Remarkably, known SG inducers include proteins associated with neurological diseases such as FMRP, SMN1, DISC1, TIA-1, TIAR and angiogenin (64–69). Cell type-dependent differences in the properties

of RNA granules might be another general issue to be elucidated.

SUPPLEMENTARY DATA

Supplementary Data are available at NAR Online.

ACKNOWLEDGEMENTS

FUNDING

REFERENCES

1. Rabbitts,T.H., Forster,A., Larson,R. and Nathan,P. (1993) Fusion of the dominant negative transcription regulator CHOP with a novel gene FUS by translocation t(12;16) in malignant liposarcoma. *Nat. Genet.*, **4**, 175–180.
2. Ichikawa,H., Shimizu,K., Hayashi,Y. and Ohki,M. (1994) An RNA-binding protein gene, TLS/FUS, is fused to ERG in human myeloid leukemia with t(16;21) chromosomal translocation. *Cancer Res.*, **54**, 2865–2868.
3. Crozat,A., Aman,P., Mandahl,N. and Ron,D. (1993) Fusion of CHOP to a novel RNA-binding protein in human myxoid liposarcoma. *Nature*, **363**, 640–644.
4. Zinszner,H., Albalat,R. and Ron,D. (1994) A novel effector domain from the RNA-binding protein TLS or EWS is required for oncogenic transformation by CHOP. *Genes Dev.*, **8**, 2513–2526.
5. Doi,H., Okamura,K., Bauer,P.O., Furukawa,Y., Shimizu,H., Kurosawa,M., Machida,Y., Miyazaki,H., Mitsui,K., Kuroiwa,Y. *et al.* (2008) RNA-binding protein TLS is a major nuclear aggregate-interacting protein in huntingtin exon 1 with expanded polyglutamine-expressing cells. *J. Biol. Chem.*, **283**, 6489–6500.
6. Woulfe,J., Gray,D.A. and Mackenzie,I.R. (2010) FUS-immunoreactive intranuclear inclusions in neurodegenerative disease. *Brain Pathol.*, **20**, 589–597.
7. Doi,H., Koyano,S., Suzuki,Y., Nukina,N. and Kuroiwa,Y. (2010) The RNA-binding protein FUS/TLS is a common aggregate-interacting protein in polyglutamine diseases. *Neurosci. Res.*, **66**, 131–133.
8. Kwiatkowski,T.J. Jr, Bosco,D.A., Leclerc,A.L., Tamrazian,E., Vanderburg,C.R., Russ,C., Davis,A., Gilchrist,J., Kasarskis,E.J., Munsat,T. *et al.* (2009) Mutations in the FUS/TLS gene on

chromosome 16 cause familial amyotrophic lateral sclerosis. *Science*, **323**, 1205–1208.
9. Vance,C., Rogelj,B., Hortobagyi,T., De Vos,K.J., Nishimura,A.L., Sreedharan,J., Hu,X., Smith,B., Ruddy,D., Wright,P. *et al.* (2009) Mutations in FUS, an RNA processing protein, cause familial amyotrophic lateral sclerosis type 6. *Science*, **323**, 1208–1211.
10. Lagier-Tourenne,C., Polymenidou,M. and Cleveland,D.W. (2010) TDP-43 and FUS/TLS: emerging roles in RNA processing and neurodegeneration. *Hum. Mol. Genet.*, **19**, R46–R64.
11. Lee,B.J., Cansizoglu,A.E., Suel,K.E., Louis,T.H., Zhang,Z. and Chook,Y.M. (2006) Rules for nuclear localization sequence recognition by karyopherin beta 2. *Cell*, **126**, 543–558.
12. Neumann,M., Roeber,S., Kretzschmar,H.A., Rademakers,R., Baker,M. and Mackenzie,I.R. (2009) Abundant FUS-immunoreactive pathology in neuronal intermediate filament inclusion disease. *Acta Neuropathol.*, **118**, 605–616.
13. Neumann,M., Rademakers,R., Roeber,S., Baker,M., Kretzschmar,H.A. and Mackenzie,I.R. (2009) A new subtype of frontotemporal lobar degeneration with FUS pathology. *Brain*, **132**, 2922–2931.
14. Munoz,D.G., Neumann,M., Kusaka,H., Yokota,O., Ishihara,K., Terada,S., Kuroda,S. and Mackenzie,I.R. (2009) FUS pathology in basophilic inclusion body disease. *Acta Neuropathol.*, **118**, 617–627.
15. Mackenzie,I.R., Neumann,M., Bigio,E.H., Cairns,N.J., Alafuzoff,I., Kril,J., Kovacs,G.G., Ghetti,B., Halliday,G., Holm,I.E. *et al.* (2010) Nomenclature and nosology for neuropathologic subtypes of frontotemporal lobar degeneration: an update. *Acta Neuropathol.*, **119**, 1–4.
16. Neumann,M., Sampathu,D.M., Kwong,L.K., Truax,A.C., Micsenyi,M.C., Chou,T.T., Bruce,J., Schuck,T., Grossman,M., Clark,C.M. *et al.* (2006) Ubiquitinated TDP-43 in frontotemporal lobar degeneration and amyotrophic lateral sclerosis. *Science*, **314**, 130–133.
17. Sreedharan,J., Blair,I.P., Tripathi,V.B., Hu,X., Vance,C., Rogelj,B., Ackerley,S., Durnall,J.C., Williams,K.L., Buratti,E. *et al.* (2008) TDP-43 mutations in familial and sporadic amyotrophic lateral sclerosis. *Science*, **319**, 1668–1672.
18. Kabashi,E., Valdmanis,P.N., Dion,P., Spiegelman,D., McConkey,B.J., Vande Velde,C., Bouchard,J.P., Lacomblez,L., Pochigaeva,K., Salachas,F. *et al.* (2008) TARDBP mutations in individuals with sporadic and familial amyotrophic lateral sclerosis. *Nat. Genet.*, **40**, 572–574.
19. Neumann,M., Mackenzie,I.R., Cairns,N.J., Boyer,P.J., Markesbery,W.R., Smith,C.D., Taylor,J.P., Kretzschmar,H.A., Kimonis,V.E. and Forman,M.S. (2007) TDP-43 in the ubiquitin pathology of frontotemporal dementia with VCP gene mutations. *J. Neuropathol. Exp. Neurol.*, **66**, 152–157.
20. Deng,H.X., Zhai,H., Bigio,E.H., Yan,J., Fecto,F., Ajroud,K., Mishra,M., Ajroud-Driss,S., Heller,S., Sufit,R. *et al.* (2010) FUS-immunoreactive inclusions are a common feature in sporadic and non-SOD1 familial amyotrophic lateral sclerosis. *Ann. Neurol.*, **67**, 739–748.
21. Lerga,A., Hallier,M., Delva,L., Orvain,C., Gallais,I., Marie,J. and Moreau-Gachelin,F. (2001) Identification of an RNA binding specificity for the potential splicing factor TLS. *J. Biol. Chem.*, **276**, 6807–6816.
22. Iko,Y., Kodama,T.S., Kasai,N., Oyama,T., Morita,E.H., Muto,T., Okumura,M., Fujii,R., Takumi,T., Tate,S. *et al.* (2004) Domain architectures and characterization of an RNA-binding protein, TLS. *J. Biol. Chem.*, **279**, 44834–44840.
23. Kuroda,M., Sok,J., Webb,L., Baechtold,H., Urano,F., Yin,Y., Chung,P., de Rooij,D.G., Akhmedov,A., Ashley,T. *et al.* (2000) Male sterility and enhanced radiation sensitivity in TLS(-/-) mice. *EMBO J.*, **19**, 453–462.
24. Hicks,G.G., Singh,N., Nashabi,A., Mai,S., Bozek,G., Klewes,L., Arapovic,D., White,E.K., Koury,M.J., Oltz,E.M. *et al.* (2000) Fus deficiency in mice results in defective B-lymphocyte development and activation, high levels of chromosomal instability and perinatal death. *Nat. Genet.*, **24**, 175–179.
25. Fujii,R., Okabe,S., Urushido,T., Inoue,K., Yoshimura,A., Tachibana,T., Nishikawa,T., Hicks,G.G. and Takumi,T. (2005) The RNA binding protein TLS is translocated to dendritic spines

by mGluR5 activation and regulates spine morphology. *Curr. Biol.*, **15**, 587–593.

26. Ou,S.H., Wu,F., Harrich,D., Garcia-Martinez,L.F. and Gaynor,R.B. (1995) Cloning and characterization of a novel cellular protein, TDP-43, that binds to human immunodeficiency virus type 1 TAR DNA sequence motifs. *J. Virol.*, **69**, 3584–3596.

27. Buratti,E., Dork,T., Zuccato,E., Pagani,F., Romano,M. and Baralle,F.E. (2001) Nuclear factor TDP-43 and SR proteins promote in vitro and in vivo CFTR exon 9 skipping. *EMBO J.*, **20**, 1774–1784.

28. Rabin,S.J., Kim,J.M., Baughn,M., Libby,R.T., Kim,Y.J., Fan,Y., La Spada,A., Stone,B. and Ravits,J. (2010) Sporadic ALS has compartment-specific aberrant exon splicing and altered cell-matrix adhesion biology. *Hum. Mol. Genet.*, **19**, 313–328.

29. Camats,M., Guil,S., Kokolo,M. and Bach-Elias,M. (2008) P68 RNA helicase (DDX5) alters activity of cis- and trans-acting factors of the alternative splicing of H-Ras. *PLoS ONE*, **3**, e2926.

30. Hallier,M., Lerga,A., Barnache,S., Tavitian,A. and Moreau-Gachelin,F. (1998) The transcription factor Spi-1/PU.1 interacts with the potential splicing factor TLS. *J. Biol. Chem.*, **273**, 4838–4842.

31. Yang,L., Embree,L.J., Tsai,S. and Hickstein,D.D. (1998) Oncoprotein TLS interacts with serine-arginine proteins involved in RNA splicing. *J. Biol. Chem.*, **273**, 27761–27764.

32. Delva,L., Gallais,I., Guillouf,C., Denis,N., Orvain,C. and Moreau-Gachelin,F. (2004) Multiple functional domains of the oncoproteins Spi-1/PU.1 and TLS are involved in their opposite splicing effects in erythroleukemic cells. *Oncogene*, **23**, 4389–4399.

33. Machida,Y., Okada,T., Kurosawa,M., Oyama,F., Ozawa,K. and Nukina,N. (2006) rAAV-mediated shRNA ameliorated neuropathology in Huntington disease model mouse. *Biochem. Biophys. Res. Commun.*, **343**, 190–197.

34. Carninci,P., Kasukawa,T., Katayama,S., Gough,J., Frith,M.C., Maeda,N., Oyama,R., Ravasi,T., Lenhard,B., Wells,C. *et al.* (2005) The transcriptional landscape of the mammalian genome. *Science*, **309**, 1559–1563.

35. Kino,Y., Washizu,C., Oma,Y., Onishi,H., Nezu,Y., Sasagawa,N., Nukina,N. and Ishiura,S. (2009) MBNL and CELF proteins regulate alternative splicing of the skeletal muscle chloride channel CLCN1. *Nucleic Acids Res.*, **37**, 6477–6490.

36. la Cour,T., Kiemer,L., Molgaard,A., Gupta,R., Skriver,K. and Brunak,S. (2004) Analysis and prediction of leucine-rich nuclear export signals. *Protein Eng. Des. Sel.*, **17**, 527–536.

37. Cansizoglu,A.E., Lee,B.J., Zhang,Z.C., Fontoura,B.M. and Chook,Y.M. (2007) Structure-based design of a pathway-specific nuclear import inhibitor. *Nat. Struct. Mol. Biol.*, **14**, 452–454.

38. Kosugi,S., Hasebe,M., Entani,T., Takayama,S., Tomita,M. and Yanagawa,H. (2008) Design of peptide inhibitors for the importin alpha/beta nuclear import pathway by activity-based profiling. *Chem. Biol.*, **15**, 940–949.

39. Andersson,M.K., Stahlberg,A., Arvidsson,Y., Olofsson,A., Semb,H., Stenman,G., Nilsson,O. and Aman,P. (2008) The multifunctional FUS, EWS and TAF15 proto-oncoproteins show cell type-specific expression patterns and involvement in cell spreading and stress response. *BMC Cell Biol.*, **9**, 37.

40. Anderson,P. and Kedersha,N. (2008) Stress granules: the Tao of RNA triage. *Trends Biochem. Sci.*, **33**, 141–150.

41. Kedersha,N., Chen,S., Gilks,N., Li,W., Miller,I.J., Stahl,J. and Anderson,P. (2002) Evidence that ternary complex (eIF2-GTP-tRNA(i)(Met))-deficient preinitiation complexes are core constituents of mammalian stress granules. *Mol. Biol. Cell*, **13**, 195–210.

42. Dang,Y., Kedersha,N., Low,W.K., Romo,D., Gorospe,M., Kaufman,R., Anderson,P. and Liu,J.O. (2006) Eukaryotic initiation factor 2alpha-independent pathway of stress granule induction by the natural product pateamine A. *J. Biol. Chem.*, **281**, 32870–32878.

43. Kedersha,N., Cho,M.R., Li,W., Yacono,P.W., Chen,S., Gilks,N., Golan,D.E. and Anderson,P. (2000) Dynamic shuttling of TIA-1 accompanies the recruitment of mRNA to mammalian stress granules. *J. Cell Biol.*, **151**, 1257–1268.

44. Eulalio,A., Behm-Ansmant,I. and Izaurralde,E. (2007) P bodies: at the crossroads of post-transcriptional pathways. *Nat. Rev. Mol. Cell Biol.*, **8**, 9–22.

45. Zhou,F.F., Xue,Y., Chen,G.L. and Yao,X. (2004) GPS: a novel group-based phosphorylation predicting and scoring method. *Biochem. Biophys. Res. Commun.*, **325**, 1443–1448.

46. Zinszner,H., Immanuel,D., Yin,Y., Liang,F.X. and Ron,D. (1997) A topogenic role for the oncogenic N-terminus of TLS: nucleolar localization when transcription is inhibited. *Oncogene*, **14**, 451–461.

47. Gregory,R.I., Yan,K.P., Amuthan,G., Chendrimada,T., Doratotaj,B., Cooch,N. and Shiekhattar,R. (2004) The microprocessor complex mediates the genesis of microRNAs. *Nature*, **432**, 235–240.

48. Shiohama,A., Sasaki,T., Noda,S., Minoshima,S. and Shimizu,N. (2007) Nucleolar localization of DGCR8 and identification of eleven DGCR8-associated proteins. *Exp. Cell Res.*, **313**, 4196–4207.

49. Wang,X., Arai,S., Song,X., Reichart,D., Du,K., Pascual,G., Tempst,P., Rosenfeld,M.G., Glass,C.K. and Kurokawa,R. (2008) Induced ncRNAs allosterically modify RNA-binding proteins in cis to inhibit transcription. *Nature*, **454**, 126–130.

50. Perrotti,D., Bonatti,S., Trotta,R., Martinez,R., Skorski,T., Salomoni,P., Grassilli,E., Lozzo,R.V., Cooper,D.R. and Calabretta,B. (1998) TLS/FUS, a pro-oncogene involved in multiple chromosomal translocations, is a novel regulator of BCR/ABL-mediated leukemogenesis. *EMBO J.*, **17**, 4442–4455.

51. Perrotti,D., Iervolino,A., Cesi,V., Cirinna,M., Lombardini,S., Grassilli,E., Bonatti,S., Claudio,P.P. and Calabretta,B. (2000) BCR-ABL prevents c-jun-mediated and proteasome-dependent FUS (TLS) proteolysis through a protein kinase CbetaII-dependent pathway. *Mol. Cell. Biol.*, **20**, 6159–6169.

52. Klint,P., Hellman,U., Wernstedt,C., Aman,P., Ron,D. and Claesson-Welsh,L. (2004) Translocated in liposarcoma (TLS) is a substrate for fibroblast growth factor receptor-1. *Cell Signal*, **16**, 515–520.

53. Gardiner,M., Toth,R., Vandermoere,F., Morrice,N.A. and Rouse,J. (2008) Identification and characterization of FUS/TLS as a new target of ATM. *Biochem. J.*, **415**, 297–307.

54. Oh,S.M., Liu,Z., Okada,M., Jang,S.W., Liu,X., Chan,C.B., Luo,H. and Ye,K. (2010) Ebp1 sumoylation, regulated by TLS/FUS E3 ligase, is required for its anti-proliferative activity. *Oncogene*, **29**, 1017–1030.

55. Rappsilber,J., Friesen,W.J., Paushkin,S., Dreyfuss,G. and Mann,M. (2003) Detection of arginine dimethylated peptides by parallel precursor ion scanning mass spectrometry in positive ion mode. *Anal. Chem.*, **75**, 3107–3114.

56. Araya,N., Hiraga,H., Kako,K., Arao,Y., Kato,S. and Fukamizu,A. (2005) Transcriptional down-regulation through nuclear exclusion of EWS methylated by PRMT1. *Biochem. Biophys. Res. Commun.*, **329**, 653–660.

57. Serman,A., Le Roy,F., Aigueperse,C., Kress,M., Dautry,F. and Weil,D. (2007) GW body disassembly triggered by siRNAs independently of their silencing activity. *Nucleic Acids Res.*, **35**, 4715–4727.

58. Fujita,K., Ito,H., Nakano,S., Kinoshita,Y., Wate,R. and Kusaka,H. (2008) Immunohistochemical identification of messenger RNA-related proteins in basophilic inclusions of adult-onset atypical motor neuron disease. *Acta Neuropathol.*, **116**, 439–445.

59. Kedersha,N., Stoecklin,G., Ayodele,M., Yacono,P., Lykke-Andersen,J., Fritzler,M.J., Scheuner,D., Kaufman,R.J., Golan,D.E. and Anderson,P. (2005) Stress granules and processing bodies are dynamically linked sites of mRNP remodeling. *J. Cell Biol.*, **169**, 871–884.

60. Kanai,Y., Dohmae,N. and Hirokawa,N. (2004) Kinesin transports RNA: isolation and characterization of an RNA-transporting granule. *Neuron*, **43**, 513–525.

61. Fujii,R. and Takumi,T. (2005) TLS facilitates transport of mRNA encoding an actin-stabilizing protein to dendritic spines. *J. Cell Sci.*, **118**, 5755–5765.

62. Yoshimura,A., Fujii,R., Watanabe,Y., Okabe,S., Fukui,K. and Takumi,T. (2006) Myosin-Va facilitates the accumulation of mRNA/protein complex in dendritic spines. *Curr. Biol.*, **16**, 2345–2351.

63. Dormann,D., Rodde,R., Edbauer,D., Bentmann,E., Fischer,I., Hruscha,A., Than,M.E., Mackenzie,I.R., Capell,A., Schmid,B.

et al. (2010) ALS-associated fused in sarcoma (FUS) mutations disrupt Transportin-mediated nuclear import. *EMBO J.*, **29**, 2841–2857.

64. Mazroui,R., Huot,M.E., Tremblay,S., Filion,C., Labelle,Y. and Khandjian,E.W. (2002) Trapping of messenger RNA by Fragile X Mental Retardation protein into cytoplasmic granules induces translation repression. *Hum. Mol. Genet.*, **11**, 3007–3017.

65. Hua,Y. and Zhou,J. (2004) Survival motor neuron protein facilitates assembly of stress granules. *FEBS Lett.*, **572**, 69–74.

66. Ogawa,F., Kasai,M. and Akiyama,T. (2005) A functional link between Disrupted-In-Schizophrenia 1 and the eukaryotic translation initiation factor 3. *Biochem. Biophys. Res. Commun.*, **338**, 771–776.

67. Furukawa,Y., Kaneko,K., Matsumoto,G., Kurosawa,M. and Nukina,N. (2009) Cross-seeding fibrillation of Q/N-rich proteins offers new pathomechanism of polyglutamine diseases. *J. Neurosci.*, **29**, 5153–5162.

68. Lu,L., Wang,S., Zheng,L., Li,X., Suswam,E.A., Zhang,X., Wheeler,C.G., Nabors,L.B., Filippova,N. and King,P.H. (2009) Amyotrophic lateral sclerosis-linked mutant SOD1 sequesters Hu antigen R (HuR) and TIA-1-related protein (TIAR): implications for impaired post-transcriptional regulation of vascular endothelial growth factor. *J. Biol. Chem.*, **284**, 33989–33998.

69. Emara,M.M., Ivanov,P., Hickman,T., Dawra,N., Tisdale,S., Kedersha,N., Hu,G.F. and Anderson,P. (2010) Angiogenin-induced tRNA-derived stress-induced RNAs promote stress-induced stress granule assembly. *J. Biol. Chem.*, **285**, 10959–10968.